INTERNATIONAL JOURNAL FOR NUMERICAL METHODS IN FLUIDS
Int. J. Numer. Meth. Fluids 2003; **42**:211–231 (DOI: 10.1002/fld.513)

Efficient discretization of pressure-correction equations on non-orthogonal grids

T. Lehnhäuser*,† and M. Schäfer

Department of Numerical Methods in Mechanical Engineering, Darmstadt University of Technology, Petersenstr. 30, D-64287 Darmstadt, Germany

SUMMARY

An alternative discretization of pressure-correction equations within pressure-correction schemes for the solution of the incompressible Navier–Stokes equations is introduced, which improves the convergence and robustness properties of such schemes for non-orthogonal grids. As against standard approaches, where the non-orthogonal terms usually are just neglected, the approach allows for a simplification of the pressure-correction equation to correspond to 5-point or 7-point computational molecules in two or three dimensions, respectively, but still incorporates the effects of non-orthogonality. As a result a wide range (including rather high values) of underrelaxation factors can be used, resulting in an increased overall performance of the underlying pressure-correction schemes. Within this context, a second issue of the paper is the investigation of the accuracy to which the pressure-correction equation should be solved in each pressure-correction iteration. The scheme is investigated for standard test cases and, in order to show its applicability to practical flow problems, for a more complex configuration of a micro heat exchanger. Copyright © 2003 John Wiley & Sons, Ltd.

KEY WORDS: finite-volume method; pressure-correction method (SIMPLE); non-orthogonal; colocated grids

1. INTRODUCTION

The numerical simulation of incompressible flows based on the Navier–Stokes equations requires special attention for the coupling of pressure and velocity fields. Pressure-correction methods like the well-known SIMPLE algorithm of Patankar and Spalding [1] are frequently employed to solve the corresponding system of discrete equations resulting from finite-volume or finite-element discretization. The basic idea of these methods, which meanwhile exist in a number of variants, is to solve first the momentum equations with an estimated pressure field for a preliminary velocity and, afterwards, the mass conservation equation is employed

* Correspondence to: T. Lehnhäuser, Dept. of Numerical Methods in Mechanical Engineering, Darmstadt University of Technology, Petersenstr. 30, D-64287 Darmstadt, Germany.
† E-mail: thomas@fnb.tu-darmstadt.de

Contract/grant sponsor: Deutsche Forschungsgemeinschaft; contract/grant number: SFB 568.

Received 26 May 2002
Revised 23 December 2002

to assemble an equation for a pressure-correction yielding corrections for the pressure and the velocity to satisfy the mass conservation. This procedure is repeated until convergence is achieved.

One crucial part of such methods is the pressure-correction equation. On orthogonal grids together with an usual second-order discretization the structure of this equation corresponds to 5-point or 7-point computational molecules in two or three dimensions, respectively. For non-orthogonal grids the structure becomes more complex, e.g. a 9-point/19-point computational molecule in two/three dimensions. The storage and solution procedure for such kinds of matrices is seen to be too complex or too expensive by many authors, especially for the three-dimensional case. Therefore, it is common practice to simplify the equation by omitting the effects of non-orthogonality entirely to obtain a 5-point or 7-point molecule again, see for example References [2–4]. However, it can be shown that on highly non-orthogonal grids these simplifications lead to deteriorated convergence behaviour of the overall pressure-correction scheme. As a consequence one has to use rather small underrelaxation factors resulting in large iteration numbers and high computational effort. For instance, for a two-dimensional set-up Perić [5] has investigated the simplified pressure-correction equation approach and found such rather poor convergence and stability behaviour on severely non-orthogonal grids. Therefore, he recommended to use the simplified scheme on slightly non-orthogonal grids, because it requires less memory and less computational effort compared to the full equation. For highly non-orthogonal grids he proposed to employ the full equation, which, however, in particular in three dimensions, is very expensive to be stored and solved. Cho and Chung [6] proposed a way of incorporating effects of non-orthogonality in the pressure-correction equation without extending the computational molecule. Unfortunately, the performance of their approach is depending on an additional user defined parameter. Regarding the number of already existing adjustable parameters in fluid flow computations this is undesirable. Additionally, for orthogonal grids the scheme cannot compete with the simplified method for certain combination of underrelaxation parameters.

The main objective of the present paper is the formulation of a discrete pressure-correction equation, which also is simplified to 5-point or 7-point computational molecules, but still incorporates the effects of non-orthogonality. Moreover, for orthogonal grids the formulation is identical to the simplified pressure-correction equation and, thus, having the same convergence properties in this case. The key idea to achieve this, is the use of an alternative approximation of pressure derivatives based on a multi-dimensional Taylor expansion as it was already introduced by Lehnhäuser and Schäfer [7] in the context of flux interpolation on distorted grids.

2. GOVERNING EQUATIONS AND DISCRETIZATION

We consider a laminar steady flow of an incompressible Newtonian fluid in an arbitrary three-dimensional domain described by the well-known Navier–Stokes equations:

$$\frac{\partial u_i}{\partial x_i} = 0 \tag{1}$$

$$u_j \frac{\partial u_i}{\partial x_j} = \frac{\partial}{\partial x_j}\left[\nu\left(\frac{\partial u_i}{\partial x_j} + \frac{\partial u_j}{\partial x_i}\right)\right] - \frac{1}{\rho}\frac{\partial p}{\partial x_i} \tag{2}$$

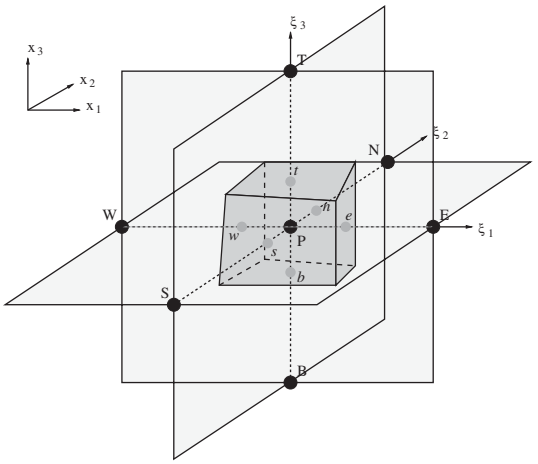

Figure 1. Arbitrary hexagonal control volume (neighbouring points are labelled according to the compass notation).

where u_i are the velocity vector components with respect to the Cartesian co-ordinates x_i, p is the pressure, ν is the kinematic viscosity and ρ is the density (for simplicity, ν and ρ are assumed to be constant).

In order to discretize the conservation Equations (1) and (2) a finite-volume method for general non-orthogonal grids is employed, which is described in detail in References [3, 8, 9]. Here we just recall some basics which will be necessary for the following considerations.

Integrating Equations (1) and (2) over an arbitrary hexahedral control volume (CV, see Figure 1) and applying the Gaussian theorem yields:

$$\sum_c \underbrace{\int_{S_c} u_i n_i \, \mathrm{d}S_c}_{\dot{m}_c} = 0 \tag{3}$$

$$\sum_c \underbrace{\int_{S_c} u_j u_i n_j \, \mathrm{d}S_c}_{F^C_{i,c}} = \sum_c \underbrace{\int_{S_c} \nu \left(\frac{\partial u_i}{\partial x_j} + \frac{\partial u_j}{\partial x_i} \right) n_j \, \mathrm{d}S_c}_{F^D_{i,c}} - \underbrace{\int_V \frac{1}{\rho} \frac{\partial p}{\partial x_i} \, \mathrm{d}V}_{S_i^p} \tag{4}$$

where the summation is performed over the six faces S_c of the hexagonal control volume ($c = e, w, n, s, t, b$). The volume integral over the pressure term S_i^p is approximated by the three-dimensional midpoint rule yielding

$$S_i^p \approx \frac{1}{\rho} \left(\frac{\partial p}{\partial x_i} \right)_P \delta V \tag{5}$$

where δV is the volume of the corresponding CV. The mass fluxes $\dot{m}_c$, the convective fluxes $F^C_{i,c}$ and the diffusive fluxes $F^D_{i,c}$ are approximated for each face separately by the

two-dimensional midpoint rule, which, e.g. for the east face, yields

$$\dot{m}_e \approx \overline{(u_i)}_e n_i \delta S_e \tag{6}$$

$$F_{i,e}^C \approx \dot{m}_e \overline{(u_i)}_e \tag{7}$$

$$F_{i,e}^D \approx \nu \left(\left(\frac{\partial u_i}{\partial x_j} \right)_e + \left(\frac{\partial u_j}{\partial x_i} \right)_e \right) n_j \delta S_e \tag{8}$$

where δS_e denotes the area of the east face. Here and in the following, the overbar denotes an appropriate interpolation of the cell face value by the nodal values.

A major concern of this paper is the derivative approximation on non-orthogonal and distorted grids. Thus, we will discuss the discretization of the derivatives in the pressure term (5) and the diffusive fluxes (8) separately in the next section. To proceed with the description of the algorithm we consider that the discretized momentum equations can be written in the following form:

$$a_P^{u_i} u_{i,P} + \sum_C a_C^{u_i} u_{i,C} = b^{u_i} \tag{9}$$

where $C = E, W, N, S, T, B$ denotes the midpoint of the neighbouring CVs. $a_P^{u_i}, a_C^{u_i}$ represent the corresponding coefficients and b^{u_i} the source terms of the discrete u_i-equation.

To solve the coupled system of discrete equations an iterative pressure-correction technique of SIMPLE type (see Patankar and Spalding [1]) is employed. Here, we omit an extensive description of the applied procedure which can be found in, e.g. Ferziger and Perić [10] and provide an outline only.

The solution procedure consists of two main steps which makes one SIMPLE iteration. At first, provisional velocity components u_i^* are computed by evaluating the discrete momentum equation (9) with an estimated pressure field p^*. Calculating the mass fluxes $\dot{m}_c^*$ with these velocities the continuity equation is not fulfilled but leaving an artificial mass source b_m for each CV:

$$b_m = \sum_c \dot{m}_c^*(u_c^*, v_c^*) \tag{10}$$

Then corrections u_i' and p' to u_i^* and p^*, respectively, are sought such that the corrected values exactly fulfil the discrete continuity equation. Subtracting Equation (10) from Equation (3) yields an equation for the mass flux correction which is a function of the velocity corrections:

$$\sum_c \dot{m}_c'(u_c', v_c') = -b_m \tag{11}$$

In the spirit of the SIMPLE algorithm from the momentum equations the following expressions for the velocity corrections can be derived:

$$u_{i,P}' = -\frac{\delta V}{\rho a_P^{u_i}} \left(\frac{\partial p'}{\partial x_i} \right)_P \tag{12}$$

To determine the correction at the CV faces without introducing oscillations due to the colocated grid arrangement the selective interpolation technique of Rhie and Chow [11] is

employed, which reads:

$$u'_{i,e} = -\overline{\left(\frac{\delta V}{\rho a_P^{u_i}}\right)_e}\left(\frac{\partial p'}{\partial x_i}\right)_e \tag{13}$$

The appropriate approximation of the derivative yields the equation for the pressure correction p'. Again we refer to the next section.

For the sake of completeness we note that the artificial mass source b_m is assembled using the pressure weighted interpolation which is described in detail, for instance in Miller and Schmidt [12].

3. DERIVATIVE APPROXIMATION

To finalize the discretization we have to approximate derivatives at different locations, namely at the cell centre P (e.g. the pressure term (5)) or at the cell face centres e, w, n, s, t, b (e.g. the diffusive fluxes (8) and the correction term in Equation (13)). In case of the cell centre approximations a standard co-ordinate transformation scheme can be applied both efficiently and accurately as will be shown in the following. In case of the derivatives at a cell face centre the co-ordinate transformation scheme introduces cell corner values, which have to be interpolated. Thus, a second scheme for the approximation of the derivatives at cell faces is considered in this paper, which is based on a multi-dimensional Taylor series expansion.

3.1. Co-ordinate transformation scheme (CTS)

The co-ordinate transformation scheme expresses derivatives in the Cartesian directions x_i in terms of the local co-ordinate system $\bar{x}_i$:

$$\frac{\partial \phi(\bar{x}_j)}{\partial x_i} = \frac{\partial \phi}{\partial \bar{x}_j}\frac{\partial \bar{x}_j}{\partial x_i} = \frac{\beta^{ij}}{J}\frac{\partial \phi}{\partial \bar{x}_j} \tag{14}$$

where β^{ij} represents the cofactor of $\partial x_i/\partial \bar{x}_j$ in the Jacobian $J = \det(\partial x_i/\partial \bar{x}_j)$ of the transformation $x_i \to \bar{x}_j$.

To approximate the derivatives at the cell centre point P the auxiliary face centre points e, w, n, s, t, b are employed due to the definition of the local co-ordinate system ξ_j (see Figure 1). Finally, the discrete version of Equation (14) for the centre point P reads:

$$\left(\frac{\partial \phi}{\partial x_i}\right)_P \approx \frac{\gamma^{ji}_{P,\mathrm{CTS}}}{\mathscr{J}_{P,\mathrm{CTS}}}\Phi^j_{P,\mathrm{CTS}}, \quad i,j = 1,2,3 \tag{15}$$

with

$$\begin{aligned}
\Phi^1_{P,\mathrm{CTS}} &= (\phi_e - \phi_w)\\
\Phi^2_{P,\mathrm{CTS}} &= (\phi_n - \phi_s)\\
\Phi^3_{P,\mathrm{CTS}} &= (\phi_t - \phi_b)\\
\gamma^{1i}_{P,\mathrm{CTS}} &= \varepsilon_{ikl}[(x_{k,n} - x_{k,s})(x_{l,t} - x_{l,b})]
\end{aligned}$$

$$\gamma^{2i}_{P,\mathrm{CTS}} = \varepsilon_{ikl}[(x_{k,t} - x_{k,b})(x_{l,e} - x_{l,w})]$$
$$\gamma^{3i}_{P,\mathrm{CTS}} = \varepsilon_{ikl}[(x_{k,e} - x_{k,w})(x_{l,n} - x_{l,s})]$$
$$\mathscr{J}_{P,\mathrm{CTS}} = (x_{i,e} - x_{i,w})\gamma^{1i}_{P,\mathrm{CTS}}$$

The values of ϕ at the cell face centre points are obtained by a linear interpolation between the corresponding computational points, e.g. $\phi_e = \delta_E\phi_E + \delta_P\phi_P + \mathcal{O}(\Delta x^2)$ with appropriate interpolation factors δ_E and δ_P.

The order of the scheme is given by the leading term of the discretization error $\tau_{i,P,\mathrm{CTS}}$ of the CTS approximation. The error can be determined by investigating the corresponding Taylor series expansions around the cell centre point P for the cell face centre points, e.g.:

$$\phi_A = \phi_P + (x_{i,P} - x_{i,A})\left(\frac{\partial\phi}{\partial x_i}\right)_P + \frac{1}{2}(x_{i,P} - x_{i,A})(x_{j,P} - x_{j,A})\left(\frac{\partial^2\phi}{\partial x_i\partial x_j}\right)_P + \mathcal{O}(\Delta x^3) \tag{16}$$

with $A = e, w, n, s, t, b$. Thus, the error of the discretization for the derivative in x_i-direction reads:

$$\tau_{i,P,\mathrm{CTS}} = \frac{1}{\mathscr{J}_{P,\mathrm{CTS}}}[\zeta_{ew}\gamma^{1i}_{P,\mathrm{CTS}} + \zeta_{ns}\gamma^{2i}_{P,\mathrm{CTS}} + \zeta_{tb}\gamma^{3i}_{P,\mathrm{CTS}}] + \mathcal{O}(\Delta x^2) \tag{17}$$

with

$$\zeta_{ew} = \frac{1}{2}[(x_{k,e} - x_{k,P})(x_{l,e} - x_{l,P}) - (x_{k,w} - x_{k,P})(x_{l,w} - x_{l,P})]\left(\frac{\partial^2\phi}{\partial x_k\partial x_l}\right)_P$$
$$\zeta_{ns} = \frac{1}{2}[(x_{k,n} - x_{k,P})(x_{l,n} - x_{l,P}) - (x_{k,s} - x_{k,P})(x_{l,s} - x_{l,P})]\left(\frac{\partial^2\phi}{\partial x_k\partial x_l}\right)_P$$
$$\zeta_{tb} = \frac{1}{2}[(x_{k,t} - x_{k,P})(x_{l,t} - x_{l,P}) - (x_{k,b} - x_{k,P})(x_{l,b} - x_{l,P})]\left(\frac{\partial^2\phi}{\partial x_k\partial x_l}\right)_P$$

Due to the definition of a CV, the centre point P is located such that the distances between e and w, n and s, t and b, respectively, are halved. Thus, the terms $\zeta_{ew}, \zeta_{ns}, \zeta_{tb}$ vanish and the error always is of second-order.

Similarly the derivatives at the cell face centre points are approximated. The procedure is presented for the east face only. The other faces can be treated accordingly. Figure 2 indicates that the local co-ordinate system is defined by η_i. The derivative $\partial\phi/\partial\eta_1$ can be approximated by using directly the computational points P and E, while for $\partial\phi/\partial\eta_2$ and $\partial\phi/\partial\eta_3$ the auxiliary points ne, se, te, be have to be employed. Thus, one can approximate the derivatives at the east face with the CTS scheme by

$$\left(\frac{\partial\phi}{\partial x_i}\right)_e \approx \frac{\gamma^{ij}_{e,\mathrm{CTS}}}{\mathscr{J}_{e,\mathrm{CTS}}}\Phi^j_{e,\mathrm{CTS}}, \quad i,j = 1,2,3 \tag{18}$$

where

$$\Phi^1_{e,\mathrm{CTS}} = (\phi_E - \phi_P)$$
$$\Phi^2_{e,\mathrm{CTS}} = (\phi_{ne} - \phi_{se})$$

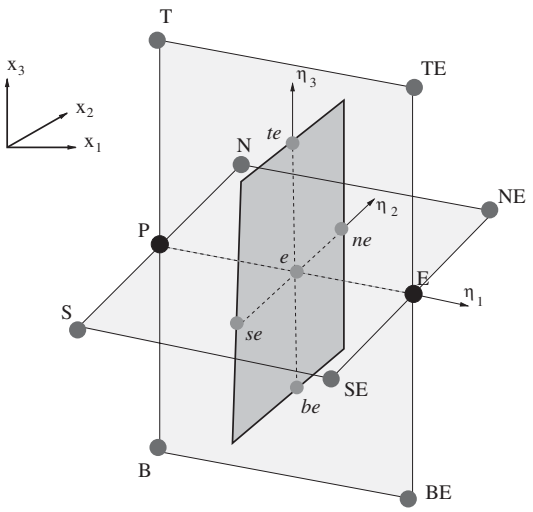

Figure 2. Arbitrary east face with the computational points P, E and auxiliary points e, ne, se, te, be.

$$\Phi^{3}_{e,\mathrm{CTS}} = (\phi_{te} - \phi_{be})$$
$$\gamma^{1i}_{e,\mathrm{CTS}} = \varepsilon_{ikl}[(x_{k,ne} - x_{k,se})(x_{l,te} - x_{l,be})]$$
$$\gamma^{2i}_{e,\mathrm{CTS}} = \varepsilon_{ikl}[(x_{k,te} - x_{k,be})(x_{l,E} - x_{l,P})]$$
$$\gamma^{3i}_{e,\mathrm{CTS}} = \varepsilon_{ikl}[(x_{k,E} - x_{k,P})(x_{l,ne} - x_{l,se})]$$
$$\mathscr{J}_{e,\mathrm{CTS}} = (x_{i,E} - x_{i,P})\gamma^{1i}_{e,\mathrm{CTS}}$$

The order of the scheme is given by the leading term of the truncation error $\tau_{i,e,\mathrm{CTS}}$. For the derivative in x_i-direction it reads:

$$\tau_{i,e,\mathrm{CTS}} = \frac{1}{2\mathscr{J}_{e,\mathrm{CTS}}}[\zeta_{EP}\gamma^{1i}_{e,\mathrm{CTS}} + \zeta_{ns}\gamma^{2i}_{e,\mathrm{CTS}} + \zeta_{tb}\gamma^{3i}_{e,\mathrm{CTS}}]\frac{\partial^2\phi}{\partial x_j^2} + \mathscr{O}(\Delta x^2) \tag{19}$$

with

$$\zeta_{EP} = \frac{1}{2}[(x_{k,E} - x_{k,e})(x_{l,E} - x_{l,e}) - (x_{k,P} - x_{k,e})(x_{l,P} - x_{l,e})]\left(\frac{\partial^2\phi}{\partial x_k \partial x_l}\right)_e$$
$$\zeta_{ns} = \frac{1}{2}[(x_{k,ne} - x_{k,e})(x_{l,ne} - x_{l,e}) - (x_{k,se} - x_{k,e})(x_{l,se} - x_{l,e})]\left(\frac{\partial^2\phi}{\partial x_k \partial x_l}\right)_e$$
$$\zeta_{tb} = \frac{1}{2}[(x_{k,te} - x_{k,e})(x_{l,te} - x_{l,e}) - (x_{k,be} - x_{k,e})(x_{l,be} - x_{l,e})]\left(\frac{\partial^2\phi}{\partial x_k \partial x_l}\right)_e$$

Again we have $\zeta_{ns} = \zeta_{tb} = 0$, due to the definition of the CV. Unfortunately, ζ_{EP} is not necessarily zero. Thus, the scheme formally is only first-order accurate. However, Ferziger and

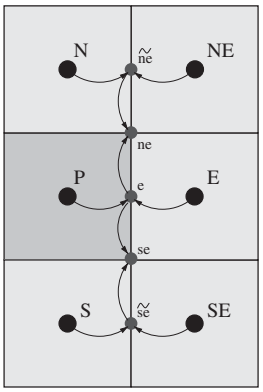

Figure 3. Interpolation of corner point values.

Perić [10] have shown that the first-order term is reduced by a factor of four or more when refining the grid spacing properly. Thus, in practice, second-order is achieved.

Finally, the values of ϕ at the cell edge centre points ne, se, te, be are approximated by bilinear interpolation. For instance, to obtain the value of ϕ at the auxiliary point ne one interpolates between P, E and N, NE first. A second interpolation then yields the sought quantity (see Figure 3). The first step again corresponds to the above mentioned standard interpolation, while the second step is never applied elsewhere. Thus, an applicable practice is to use the corresponding interpolation factors at the centre node P. On distorted grids this interpolation practice introduces additional errors of order $\mathcal{O}(\Delta x)$ which influence on the solution depends on the distortion of the grid.

The co-ordinate transformation scheme is an appropriate choice for the approximation of derivatives at cell centre points. For derivatives at face centre points this scheme shows some unwanted features such as reduced accuracy due to the interpolation. Especially when treating the pressure-correction equation there are further drawbacks. We return to this issue in Section 3.3. Before, we introduce an alternative discretization for derivatives at cell face centre points.

3.2. Derivative approximation based on multi dimensional Taylor series expansion (DABT)

A Taylor series expansion for an arbitrary point A around e in three dimensions reads:

$$\phi_A = \phi_e + (x_{i,e} - x_{i,A}) \left(\frac{\partial \phi}{\partial x_i} \right)_e + \frac{1}{2}(x_{i,e} - x_{i,A})(x_{j,e} - x_{j,A}) \left(\frac{\partial^2 \phi}{\partial x_i \partial x_j} \right)_e + \mathcal{O}(\Delta x_i^3) \tag{20}$$

Obviously, on the right-hand side the sought derivatives appear as unknowns. Neglecting the second- and higher-order terms the cell face centre value ϕ_e appears as a fourth unknown. On the left-hand side of Equation (20) we have the value of ϕ for an arbitrary point A in the vicinity of e. Thus, we can chose for A the adjacent computational points $A = P, E, N, S, T, B, NE, SE, TE, BE$, respectively. To determine the four unknowns it would be

sufficient to employ four nodes only, but for symmetry reasons we include ten nodes in the approximation. By simple algebra one obtains for every derivative an equation of the form:

$$\left(\frac{\partial\phi}{\partial x_i}\right)_e \approx \frac{\gamma^{ji}_{e,\mathrm{DABT}}}{\mathscr{J}_{e,\mathrm{DABT}}}\,\Phi^{j}_{e,\mathrm{DABT}}, \quad i,j=1,2,3 \tag{21}$$

with

$$\begin{aligned}
\Phi^{1}_{e,\mathrm{DABT}} &= (\phi_E - \phi_P)\\
\Phi^{2}_{e,\mathrm{DABT}} &= (\phi_N - \phi_S + \phi_{NE} - \phi_{SE})\\
\Phi^{3}_{e,\mathrm{DABT}} &= (\phi_T - \phi_B + \phi_{TE} - \phi_{BE})\\
\gamma^{1i}_{e,\mathrm{DABT}} &= \varepsilon_{ikl}[(x_{k,N} - x_{k,S} + x_{k,NE} - x_{k,SE})(x_{l,T} - x_{l,B} + x_{l,TE} - x_{l,BE})]\\
\gamma^{2i}_{e,\mathrm{DABT}} &= \varepsilon_{ikl}[(x_{k,T} - x_{k,B} + x_{k,TE} - x_{k,BE})(x_{l,E} - x_{l,P})]\\
\gamma^{3i}_{e,\mathrm{DABT}} &= \varepsilon_{ikl}[(x_{k,E} - x_{k,P})(x_{l,N} - x_{l,S} + x_{l,NE} - x_{l,SE})]\\
\mathscr{J}_{e,\mathrm{DABT}} &= (x_{i,E} - x_{i,P})\gamma^{1i}_{e,\mathrm{DABT}}
\end{aligned}$$

Obviously, the structure of the DABT scheme is very similar to that of the CTS scheme. However, the coefficients γ^{ji} and Φ^{j} differ and, in particular, no cell face edge points are introduced in the DABT scheme. The order of the scheme is given by the truncation error $\tau_{i,\mathrm{DABT}}$. For the derivative in x_i-direction it reads:

$$\tau_{i,\mathrm{DABT}} = \frac{1}{2\mathscr{J}_{e,\mathrm{DABT}}}\,[\zeta_{EP}\gamma^{1i}_{e,\mathrm{DABT}} + \zeta_{NS}\gamma^{2i}_{e,\mathrm{DABT}} + \zeta_{TB}\gamma^{3i}_{e,\mathrm{DABT}}]\frac{\partial^2\phi}{\partial x_j^2} + \mathscr{O}(\Delta x^2) \tag{22}$$

with

$$\begin{aligned}
\zeta_{EP} &= \frac{1}{2}[(x_{k,E} - x_{k,e})(x_{l,E} - x_{l,e}) - (x_{k,P} - x_{k,e})(x_{l,P} - x_{l,e})]\left(\frac{\partial^2\phi}{\partial x_k\partial x_l}\right)_e\\
\zeta_{NS} &= \frac{1}{2}[(x_{k,N} - x_{k,e})(x_{l,N} - x_{l,e}) - (x_{k,S} - x_{k,e})(x_{l,S} - x_{l,e})\\
&\quad + (x_{k,NE} - x_{k,e})(x_{l,NE} - x_{l,e}) - (x_{k,SE} - x_{k,e})(x_{l,SE} - x_{l,e})]\left(\frac{\partial^2\phi}{\partial x_k\partial x_l}\right)_e\\
\zeta_{TB} &= \frac{1}{2}[(x_{k,T} - x_{k,e})(x_{l,T} - x_{l,e}) - (x_{k,B} - x_{k,e})(x_{l,B} - x_{l,e})\\
&\quad + (x_{k,TE} - x_{k,e})(x_{l,TE} - x_{l,e}) - (x_{k,BE} - x_{k,e})(x_{l,BE} - x_{l,e})]\left(\frac{\partial^2\phi}{\partial x_k\partial x_l}\right)_e
\end{aligned}$$

The leading term in Equation (22) is first-order and very similar to the truncation error of the CTS scheme. Thus, following Ferziger and Perić [10], it is straightforward to show that the first-order term is reduced by a factor of four or more with grid refinement. However, the DABT scheme does not incorporate any interpolation thus avoiding additional error terms.

Note that the same derivative approximation has already been introduced by Moulinec and Wesseling [13]. Despite following a different derivation they found the same formula. In their studies they applied the scheme to the derivatives in the diffusive flux and found superior accuracy compared to the CTS scheme. Further, the derivative approximation can be employed together with the Taylor series expansion to design a multi-dimensional interpolation formula for severely distorted grids as presented in Lehnhäuser and Schäfer [7].

3.3. Discretization of the pressure-correction equation

The derivatives in the pressure-correction equation are approximated either by the CTS or the DABT scheme to yield a discrete equation of the following general form:

$$a_P p'_P + \sum_C a_C p'_C = -b_m \tag{23}$$

For a detailed derivation of the coefficients in Equation (23) we start with the equation for the mass flux correction, e.g. for the east face where we substitute the velocity corrections $u'_{i,e}$ by Equation (13):

$$\dot{m}'_e = u'_{i,e} n_i \delta S_e = -\overline{\left(\frac{\delta V}{\rho a_P^{u_i}}\right)_e} \left(\frac{\partial p'}{\partial x_i}\right)_e n_i \delta S_e \tag{24}$$

Using the CTS formula to approximate the derivative of the pressure correction yields:

$$\dot{m}'_e = -(p'_E - p'_P)\alpha^1_{\mathrm{CTS}} - (p'_{ne} - p'_{se})\alpha^2_{\mathrm{CTS}} - (p'_{te} - p'_{be})\alpha^3_{\mathrm{CTS}} \tag{25}$$

where the factors α are given by:

$$\alpha^j_{\mathrm{CTS}} = \overline{\left(\frac{\delta V}{\rho a_P^{u_i}}\right)_e} \frac{\gamma^{ji}_{e,\mathrm{CTS}}}{\mathscr{J}_{e,\mathrm{CTS}}} \delta S_e n_i$$

The values of p' at the corner points can be expressed by the cell centre values using the above mentioned twofold linear interpolation, e.g. for p'_{ne} and p'_{se}:

$$p'_{ne} = (1-\psi_1)[(1-\psi_2)p'_P + \psi_2 p'_E] + \psi_1[(1-\psi_3)p'_N + \psi_3 p'_{NE}]$$
$$p'_{se} = (1-\psi_4)[(1-\psi_5)p'_S + \psi_5 p'_{SE}] + \psi_4[(1-\psi_2)p'_P + \psi_2 p'_E]$$

with appropriate interpolation factors $\psi_i \in [0,1]$. Thus, one can write

$$\begin{aligned} p'_{ne} - p'_{se} = {} & \psi_1(1-\psi_3)p'_N + \psi_1\psi_3 p'_{NE} \\ & - (1-\psi_4)(1-\psi_5)p'_S + (1-\psi_4)\psi_5 p'_{SE} \\ & + (1-\psi_2)(1-\psi_1-\psi_4)p'_P + \psi_2(1-\psi_1-\psi_4)p'_E \end{aligned}$$

In principle one can now evaluate the coefficients a_C in Equation (23) for the CTS scheme. Nevertheless, a common simplification is to neglect entirely all contributions due to non-orthogonality, e.g. to neglect the contributions of the corner points. This is justified as long as

the procedure converges since all corrections vanish in state of convergence anyway. Moreover, that implies that the final solution is not altered by this simplification. Eventually, one can determine the corresponding matrix contribution for the east face:

$$a_P^e = \alpha_{\mathrm{CTS}}^1, \quad a_E^e = -\alpha_{\mathrm{CTS}}^1, \quad a_N^e = 0, \quad a_S^e = 0, \quad a_T^e = 0, \quad a_B^e = 0$$

Similarly one can determine the contributions of the other faces. The overall entries are determined by the sum of the corresponding contributions of all faces. In the following we will refer to this approach as the simplified pressure-correction equation (SPC).

Employing the DABT scheme the starting point is again Equation (24). The substitution of the derivatives yields:

$$\begin{aligned} \dot{m}'_e = &-(p'_E - p'_P)\alpha_{\mathrm{DABT}}^1 - (p'_{NE} - p'_{SE} + p'_N - p'_S)\alpha_{\mathrm{DABT}}^2 \\ &-(p'_{TE} - p'_{BE} + p'_T - p'_B)\alpha_{\mathrm{DABT}}^3 \end{aligned} \tag{26}$$

where the factors α are given by

$$\alpha_{\mathrm{DABT}}^j = \overline{\left(\frac{\delta V}{\rho a_P^{u_i}}\right)}_e \frac{\gamma_{e,\mathrm{DABT}}^{ji}}{\mathcal{J}_{e,\mathrm{DABT}}} \delta S_e n_i$$

Obviously no face corner point values appear in Equation (26). Thus, no interpolation is required and one can determine the matrix entries for the east face directly:

$$\begin{aligned} a_P^e &= \alpha_{\mathrm{DABT}}^1, & a_E^e &= -\alpha_{\mathrm{DABT}}^1 \\ a_N^e &= -\alpha_{\mathrm{DABT}}^2, & a_{NE}^e &= -\alpha_{\mathrm{DABT}}^2 \\ a_S^e &= \alpha_{\mathrm{DABT}}^2, & a_{SE}^e &= \alpha_{\mathrm{DABT}}^2 \\ a_T^e &= -\alpha_{\mathrm{DABT}}^3 & a_{TE}^e &= -\alpha_{\mathrm{DABT}}^3 \\ a_B^e &= \alpha_{\mathrm{DABT}}^3, & a_{BE}^e &= \alpha_{\mathrm{DABT}}^3 \end{aligned}$$

Again, the overall entries are determined by the sum of the corresponding contributions of all faces.

Obviously, the contribution of the corner neighbours cannot be treated implicitly, when one likes to have a restriction to the 7-stencil discretization. An explicit treatment when assembling the pressure-correction equation is also impossible, since there are no reasonable values for the pressure corrections. However, such values are available when the current pressure-correction equation is solved approximately by the iterative solver. Thus, a possibility is to interrupt the solver and to use the current values for the pressure correction to treat the corner neighbour contributions explicitly following the ideas of *deferred correction*-approaches. After updating the source terms correspondingly the solution procedure can be continued. Again this is justified as long as the procedure converges (see above).

Treating terms explicitly is another way of simplifying the pressure-correction equation. But in contrast to the SPC approach no terms are neglected. Thus, in the following we will refer to this approach as the (semi-)full pressure-correction equation (FPC). Observe that in case of orthogonal grids the FPC and SPC approaches are identical.

Obviously, the coefficient matrices of both methods join some common features, while they also differ in some important respects. Firstly, both methods produce a matrix which consists

of 7 diagonals. Furthermore, it is guaranteed that the centre coefficient a_P is equal to the negative sum of its neighbour coefficients which can be exploited in the computer code. On the other hand, all off-diagonal entries are negative in case of the CTS discretization while using DABT this cannot be guaranteed. Since this feature of a matrix is essential to apply an iterative solver efficiently and robustly we consider a cut-off here, e.g. all positive entries are clipped to zero, which again does not influence the converged solution since a correction equation is treated. To keep the row sum property of the matrix the clipped values are lumped to the main diagonal. However, it can be expected that the pressure-correction equation using the DABT discretization will be more challenging to the iterative solver compared to the CTS scheme.

4. NUMERICAL RESULTS

The numerical experiments intend to demonstrate the superiority of the FPC compared to the SPC scheme. Beside that, a second issue is the investigation of the solver accuracy for the pressure-correction equation and its influence on the convergence and robustness behaviour of the underlying pressure-correction method. Since we expect no influence from the dimensionality of the flow problem both investigations are carried out for the lid driven cavity problem. Though this two-dimensional test case is rather academic, it suits best for our purpose since it emphasizes the problems occurring in practical configurations. To show the applicability of the findings obtained for the test case to more complex configuration the flow through a micro heat exchanger is also investigated.

Beside the parameters which are varied for the different experiments some are kept constant for all computations. These are the overall convergence limit and the settings for the linear system solver, to mention the most important. In any case the calculation is terminated if the normed residual of every considered equation falls below the convergence limit of $\varepsilon = 1 \times 10^{-4}$. This implies that the divergence of the final velocity field is at least of the same order of magnitude. For the solution of the linear system of equations we employ the strongly implicit method (SIP) proposed by Stone [14] for the momentum as well as for the pressure-correction equations. The user supplied parameter for this method is taken to be $\alpha_{\mathrm{SIP}} = 0.5$.

4.1. Lid driven cavity

For the basic investigations of the simplified and the full pressure-correction equations we first consider the two-dimensional flow in a lid driven cavity. To show the influence of a skewed mesh we investigate two geometrical set-ups shown in Figure 4. The Reynolds number is taken to be $Re = uL/v = 100$. The spatial discretization consists of four successively refined grids with 10×10 CV on the coarsest and 80×80 CV on the finest grid. This test case was also considered by Perić [5], where he investigated the performance of a fully implicitly treated pressure-correction equation.

4.1.1. Investigation of underrelaxation parameters. In this section the influence of the underrelaxation parameter is investigated. To do so all other influencing parameters are kept constant. To be more precise the solution procedure for the correction equation is terminated

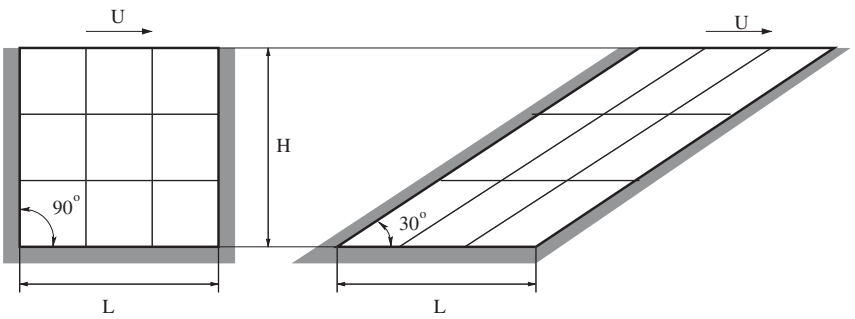

Figure 4. Geometrical configuration of the lid driven cavity problem with indicated grid.

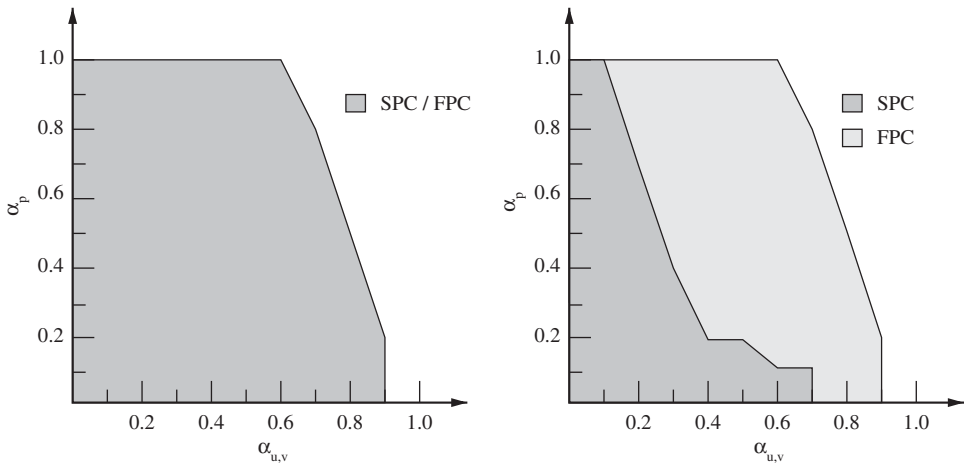

Figure 5. Influence of underrelaxation factors on the convergence behaviour for the 90°- (left) and 30°-cavity (right) using the simplified and full pressure-correction equation on a grid with 40×40 CV.

either if the sum of its absolute residual falls by a factor of 5 compared to the one of the first iteration or the number of iterations exceeds the limit of 20 which are a standard settings to our knowledge. Since the pressure-correction equation converges very slowly the accuracy limit is reached rarely. Especially, for the computations presented in this section all 20 iterations are spent in each SIMPLE iteration.

We start with the 90°-cavity where both the SPC and FPC approaches yield identical formulae. The employed computational grid is orthogonal and equidistant in both directions. Thus, one expects that the solution procedure works the best concerning the efficiency and robustness compared to other geometrical configurations. The picture on the left-hand side of Figure 5 indicates the combinations of underrelaxation factors which lead to a converging SIMPLE procedure. Apparently, a broad range of combinations can be used. Concerning the 30°-cavity (right-hand side of Figure 5) the region of possible combinations of underrelaxation

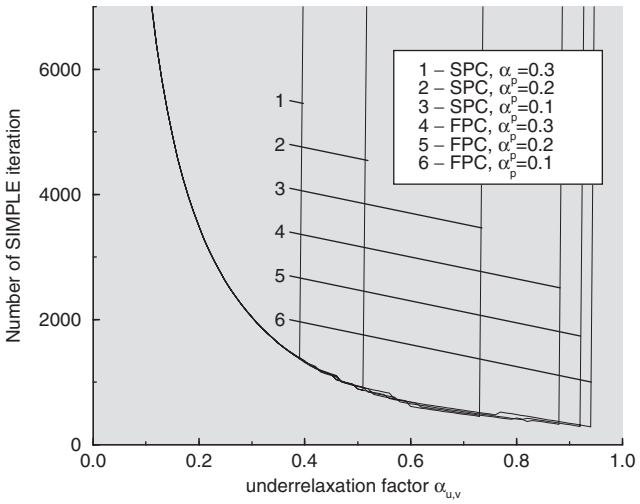

Figure 6. Dependency of the number of SIMPLE iteration on the underrelaxation factors and the pressure-correction scheme for the 30°-cavity on the grid with 80×80 CV.

factors is reduced remarkably when using the SPC scheme. The use of the FPC scheme allows to use a much broader range, which indicates that the scheme is significantly more robust than the simplified equation. The region of convergence is identical to the one found in case of the 90°-cavity which shows that the FPC approach is capable of treating the cross derivative terms correctly. To investigate the efficiency of both methods a comparison of the number of SIMPLE iterations is presented which is directly connected to the CPU time since in each SIMPLE iteration a fixed number of inner iterations are applied. For the sake of brevity only the most distinctive results are presented. Figure 6 shows the dependency of the underrelaxation factor for the momentum equations and pressure $(\alpha_{u,v}, \alpha_p)$ on the number of SIMPLE iterations. In any case the number of iterations is reduced remarkably when increasing $\alpha_{u,v}$ and keeping α_p constant whereas increasing α_p with constant $\alpha_{u,v}$ does not have any obvious effect. Nevertheless, increasing α_p bounds the maximal possible value of $\alpha_{u,v}$ more and more. In case of SPC the limitation is more restrictive than in case of FPC.

In case of convergence and constant $\alpha_{u,v}$ the SPC and the FPC approaches do not differ remarkably. However, the FPC method allows to use combinations of rather high underrelaxation factors, whereas the SPC approach diverges with such values. Thus, the overall minimum of iterations for FPC is significantly lower compared to the SPC approach. For this test case a reduction of SIMPLE iterations by 35% was realized when comparing SPC and FPC; both with the optimal combination of underrelaxation factors. The computational time is not reduced that much since it is a little more expensive to assemble the pressure-correction equation in FPC. Nevertheless, the reduction in computational time is still more than 30%.

4.1.2. Investigation of solver accuracy. Besides the underrelaxation factors other parameters in the SIMPLE algorithm influence the robustness and efficiency of the method. An interesting point is how exactly the pressure-correction equation should be solved. In contrast to the momentum equations the pressure-correction equation is rather difficult to solve because of its

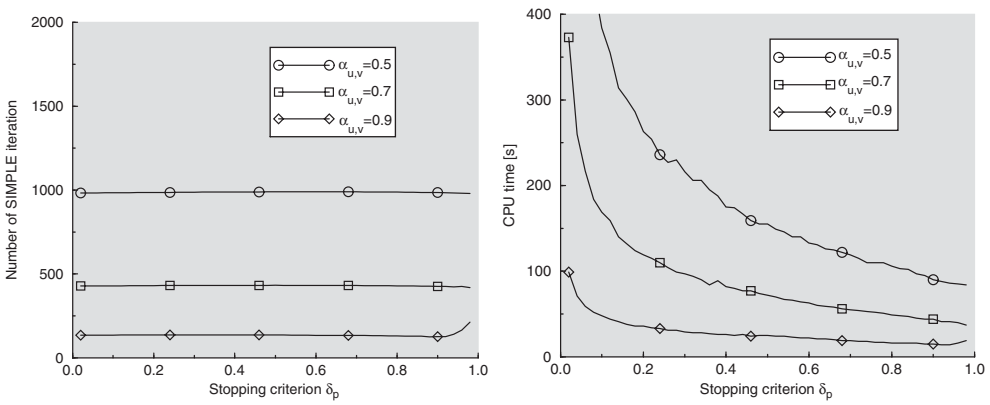

Figure 7. Influence of the stopping criterion of the linear system solver for the pressure-correction equation on the number of SIMPLE iteration and the CPU time for the 90°-cavity.

purely diffusive nature (Poisson equation with Neumann boundary conditions). On the other hand one is not interested in the exact solution of the current correction equation in every SIMPLE iteration, since the momentum equations have to be revisited anyway. Naturally, employing approximate pressure corrections does not guarantee that the divergence of the velocity field for every computational point is zero after each SIMPLE iteration. Nevertheless, if the overall method converges the divergence of the velocity tends towards zero.

In the preceding section we required that the absolute residual falls below 20% of the one of the first inner iteration or that 20 sweeps of the iterative solver are applied at most. Here, we will consider stopping criteria from 2 to 98% indicated by the parameter $\delta_p \in [0.02, 0.98]$ without limiting the number of SIP iterations. The underrelaxation factor $\alpha_p = 0.2$ is kept constant while $\alpha_{u,v}$ is varied in the range $[0.5, 0.9]$. In Figure 7 the number of SIMPLE iterations and CPU times are plotted over δ_p for the 90°-cavity. Obviously, computing the pressure correction very precisely or not does not have a big influence on the number of outer iterations. Since only a few iterations of the SIP solver are needed to compute a rough approximation, the computational time decreases when increasing δ_p. This effect is not depending on the underrelaxation factor $\alpha_{u,v}$. Nevertheless the number of SIMPLE iterations and the computational time can be reduced by choosing $\alpha_{u,v}$ close to the limit of divergence of the overall method.

Figure 8 shows the corresponding plots for the 30°-cavity using the SPC approach. For $\alpha_{u,v} = 0.5$ the situation compared to the 90°-cavity does not change significantly. Still the number of SIMPLE iterations is not affected by δ_p unless choosing very high values. Increasing the underrelaxation factor for the velocities, a lower bound for δ_p arises which is approximately 0.1 for $\alpha_{u,v} = 0.7$. For $\alpha_{u,v} = 0.9$ no computation converges at all.

Finally, Figure 9 shows the corresponding plots for the 30°-cavity using the FPC approach. The overall situation is similar to the SPC scheme. Again a lower bound for the stopping criterion is occurring. However, compared to the SPC approach the bound arises for higher underrelaxation parameters. Generally, the FPC method permits higher values for $\alpha_{u,v}$ and, therefore, one obtains faster convergence.

An interesting issue of the computations of the 30°-cavity is that there exist a lower bound for δ_p. This can be explained by the simplifications in the SPC as well as the FPC approaches.

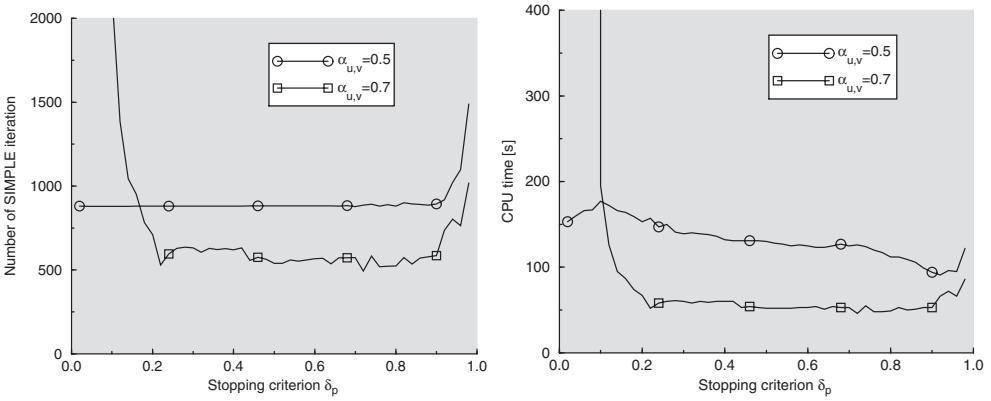

Figure 8. Influence of the stopping criterion of the linear system solver for the pressure-correction equation on the number of SIMPLE iteration and the CPU time for the 30°-cavity using the SPC scheme.

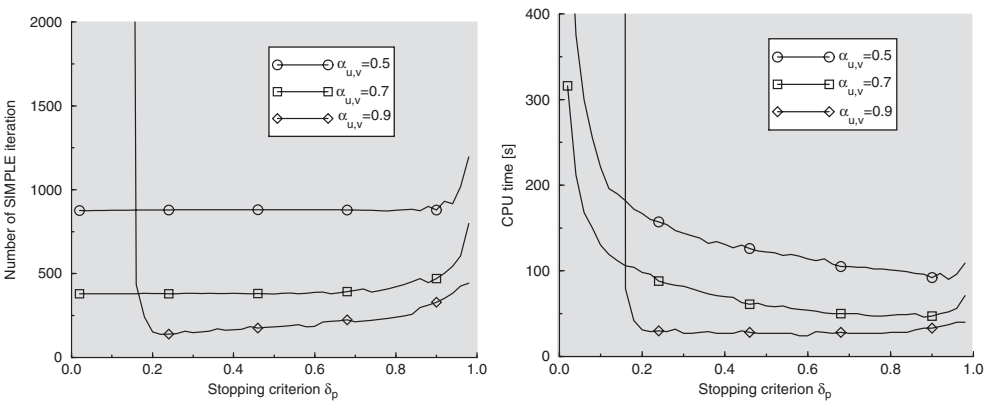

Figure 9. Influence of the stopping criterion of the linear system solver for the pressure-correction equation on the number of SIMPLE iteration and the CPU time for the 30°-cavity using the FPC scheme.

Although neglecting parts in the pressure-correction equation (SPC/FPC) or treating them explicitly (FPC) has no influence on the converged solution, it alters the pressure-correction equation of each SIMPLE iteration. Thus, the exact solution of this system does not fulfil the full pressure-correction equation (without any simplification). Consequently, if the difference between the obtained and the sought solution is too big the overall method is diverging. Naturally, this difference is depending on the applied simplification and the non-orthogonality of the grid.

The numerical experiments suggest that a kind of stabilization is introduced by solving the pressure-correction equation only roughly. A possible explanation for this behaviour is that the initial guess for the correction is always the zero field. Thus, after a few iterations of the

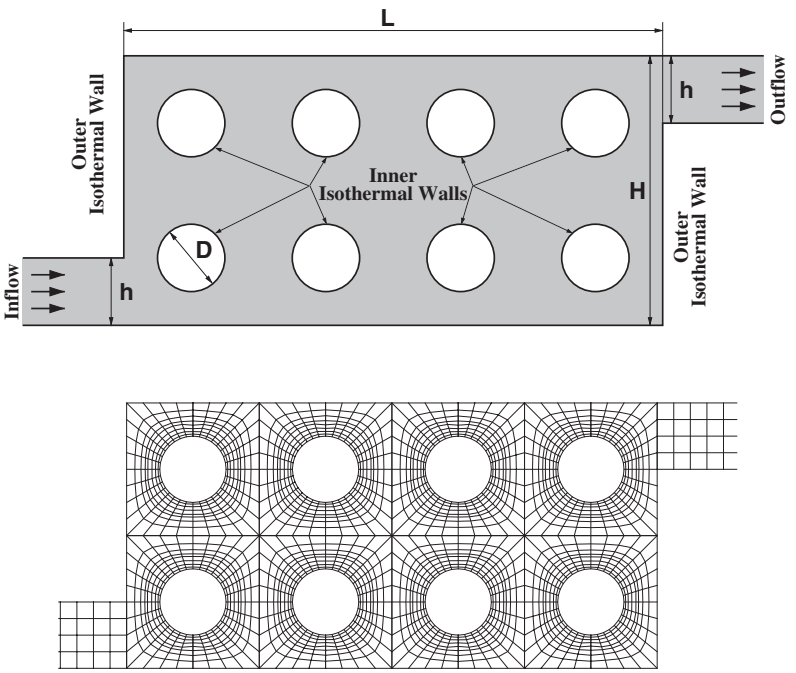

Figure 10. Geometrical configuration and a section of employed multi-block structured grid for the micro heat exchanger.

SIP solver the pressure-correction field will be not too far away from the initial estimate. If this correction is already a fairly good approximation of the pressure correction of the full correction equation the method converges. After some SIMPLE iterations the influence of the neglected parts in the simplified pressure-correction equations decreases and the calculated pressure correction becomes better and better.

The experiments also reveal that it is not necessary to compute the pressure correction very precisely concerning the efficiency of the scheme. In all investigated cases it is sufficient to reduce the absolute residual by only 2% ($\delta_p = 0.98$) to obtain a converging method. Using such high values for δ_p reduces the number of SIP iterations significantly. Since the number of SIMPLE iterations is barely affected, the fastest computations are obtained with stopping criterion $\delta_p \approx 0.9$ which is far away from the recommended standard value of 0.2. Of course, the optimal value of δ_p will be problem dependent.

4.2. Micro heat exchanger

Of course, the lid driven cavity considered in the previous sections is a rather academic test case representing hardly any practical configuration. In practice, the mesh will consist of cells with widely varying shapes and internal angles depending on the set of given boundaries. As an example of such a configuration the geometrical set-up of a heat exchanger and the associated structured grid is presented in Figure 10 (most of the numerical grid in the area of inflow and outflow has been clipped in the figure yielding a detailed view on the exchanger itself).

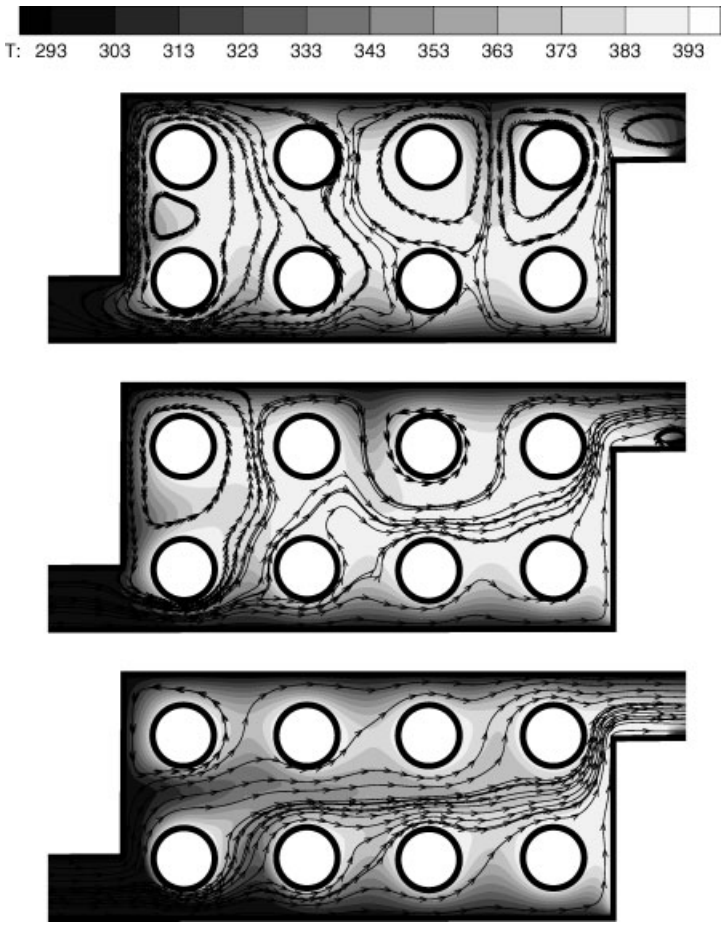

Figure 11. Visualization of the flow (streamlines) and temperature field (isothermal) of the micro heat exchanger for three Reynolds numbers. Top: $Re = 0.1$; Centre: $Re = 1$; Bottom: $Re = 10$.

Obviously, one can construct H-type grids for the inflow and outflow region. Because of the rectangular boundaries in the inflow and outflow area the grid cells are orthogonal. However, in the exchanger chamber O-type grids are employed since the inner circular boundaries of the tubes have to be approximated well. Due to the outer rectangular boundaries the O-type grids are deformed such that internal angles from 45° to 130° appear. Nevertheless, the grid quality can be considered as rather good due to grid line smoothing. Four successively refined grids are employed with 552 CV on the coarsest and 35 328 CV on the finest mesh.

The geometrical set-up used in the numerical experiments is defined by the channel height $h = 0.001$ m, the tube diameter $D = h$, the chamber lengths $L = 8h$ and the chamber height $H = 4h$. The fluid is considered to be water. The dependency of the material properties on the temperature is neglected, since they will not influence the performance of the different pressure-correction schemes. Thus, the density and the viscosity are taken to be constant.

Table I. Number of SIMPLE iterations for the micro heat exchanger at different Reynolds numbers and for different grid spacings.

CV	$Re = 0.1$			$Re = 1$			$Re = 10$		
	SPC	FPC	FPC 2	SPC	FPC	FPC 2	SPC	FPC	FPC 2
2208	134	133	265	130	130	288	100	108	255
8832	558	550	324	322	316	319	194	198	188
35328	2056	1120	439	909	504	497	538	436	446

In the numerical experiments three different Reynolds numbers $Re = hu_{\text{in}}/v_{\text{water}} = 10, 1, 0.1$ in the laminar regime are investigated, depending on the inlet (block) velocities $u_{\text{in}} = 0.01, 0.001, 0.0001$ m/s with the kinematic viscosity $v_{\text{water}} = 1 \times 10^{-6}$ m^2/s. On all outer walls a constant temperature of $T = 293$ K is prescribed whereas the inner walls possess a constant temperature of $T = 393$ K. Effects of buoyancy are modelled by the Boussinesq approximation. Although this is physically not valid for this temperature regime, the performance of the schemes to be investigated will not be affected.

To give a brief overview of the flow phenomena appearing in the exchanger chamber Figure 11 shows the streamlines and the temperature field for the different Reynolds numbers. Obviously, in case of $Re = 0.1$ the flow is mainly driven by effects of buoyancy, whereas in case of $Re = 10$ it is dominated by convection.

By transferring some of the findings of the previous section not all combinations of numerical parameters were investigated for the micro heat exchanger. First of all the SPC approach together with the standard values for the number of sweeps for the pressure-correction equation (20) and accuracy ($\delta_p = 0.2$) is applied. 3 iterations of the linear system solver are applied on the momentum equations and 5 on the energy equation without any accuracy criterion, i.e. 31 sweeps are applied in every SIMPLE iteration at most. The method also converges with underrelaxation parameters $\alpha_{u,v} = 0.9$ and $\alpha_p = 0.2$. Because lower values for $\alpha_{u,v}$ do not improve the behaviour of the scheme, results are presented only for this combination of underrelaxation factors. For comparison, the FPC method is applied with the same numerical parameters. Additionally, the FPC approach is also tested with a solver accuracy of $\delta_p = 0.8$ (FPC 2).

In Table I the number of SIMPLE iterations for the three investigated schemes for every Reynolds number are summarized. Obviously, both the SPC and FPC yield more or less the same results for the coarser grids. However, on finer grids the FPC needs fewer SIMPLE iterations compared to the SPC method. Especially for $Re = 0.1$ the difference is significant. The FPC 2 method, which solves the pressure-correction equation only very roughly, cannot compete with the other two methods on the coarse grids. Nevertheless, it profits from grid refinement and is equally good or even better on the finer grids.

To obtain a reasonable rating of the three investigated schemes it is not sufficient to consider only the number of SIMPLE iterations, since the main objective is the computing time which also depends on the number of sweeps applied in each outer iteration. Thus, the CPU time in seconds are compared in Table II. Obviously, both FPC approaches yield faster algorithms than the SPC approach. However, the difference is smaller compared to the number of outer iterations because more sweeps have to be applied to solve the pressure-correction equation

Table II. Computational time in seconds for the micro heat exchanger at different Reynolds numbers and for different grid spacings.

CV	$Re = 0.1$			$Re = 1$			$Re = 10$		
	SPC	FPC	FPC 2	SPC	FPC	FPC 2	SPC	FPC	FPC 2
2208	5.1×10^0	5.5×10^0	8.3×10^0	4.7×10^0	5.3×10^0	9.3×10^0	3.7×10^0	4.0×10^0	8.8×10^0
8832	1.0×10^2	1.1×10^2	5.2×10^1	6.0×10^1	6.4×10^1	5.4×10^1	3.9×10^1	3.6×10^1	3.6×10^1
35328	1.5×10^3	8.7×10^2	3.1×10^2	6.3×10^2	4.0×10^2	3.7×10^2	4.0×10^2	3.1×10^2	3.2×10^2

in case of the FPC approach. An additional acceleration can be achieved by raising δ_p as the results for the FPC2 method indicate. In general, the positive effects of the FPC approaches against SPC are stronger for low Reynolds numbers.

5. CONCLUSIONS

Simplifications of the pressure-correction equation to obtain a sparser matrix affects the efficiency and robustness features of pressure-correction methods. To reduce these effects an alternative discretization of the pressure-correction equation is introduced with which it is straightforward to consider parts of the cross derivative terms implicitly instead of neglecting them completely. The numerical experiments for cavity flows show that this approach is capable of yielding a robust and efficient correction method even for highly skewed configurations. Compared to the standard SPC approach the increased effort in assembling and solving the pressure-correction equation is repaid by a significantly reduced number of SIMPLE iterations and, therefore, a reduced computational time.

Considering the accuracy of the computed pressure correction in each SIMPLE iteration, the numerical experiments clearly show that it is not necessary to solve the pressure correction very accurately neither for robustness nor for efficiency of the scheme. For the investigated test case it was sufficient to reduce the absolute residual by only a few percent to obtain a converging procedure. Additionally, the number of SIMPLE iterations does not increase tremendously when using such high stopping criteria. Because of the reduced number of SIP iterations, the fastest computations are obtained with values $\delta_p > 0.7$.

Contrary to the lid driven cavity the grid for the micro heat exchanger consists of cells with a variety of different shapes. In this case the differences in performance between the proposed schemes and the standard scheme are not that distinct. Especially, the robustness of the investigated schemes does not depend that strongly on the underrelaxation parameters. Nevertheless, concerning the efficiency, the FPC approaches yield a higher convergence rate on the finer grid levels and therefore a reduced overall computing time for any investigated Reynolds number, which, however, influences the efficiency distinctly as the numerical experiments have shown.

ACKNOWLEDGEMENTS

The financial support by the *Deutsche Forschungsgemeinschaft* is gratefully acknowledged.

REFERENCES

1. Patankar SV, Spalding DB. A calculation procedure for heat, mass and momentum transfer in three dimensional parabolic flows. *International Journal of Heat and Mass Transfer* 1972; **15**:1787–1806.
2. Demirdžić I. A finite volume method for the computation of fluid flow in complex geometries. *Ph.D. thesis*, University of London, 1982.
3. Perić M. A finite volume method for the prediction of three-dimensional fluid flow in complex ducts. *Ph.D. thesis*, University of London, 1985.
4. Braaten M, Shyy W. A study of recirculating flow computation using boundary-fitted co-ordinates: Consistency aspects and mesh skewness. *Numerical Heat Transfer* 1986; **9**:559–574.
5. Perić M. Analysis of pressure-velocity coupling on nonorthogonal grids. *Numerical Heat Transfer*, *Part B* 1990; **17**:63–82.
6. Cho MJ, Chung MK. New treatment of nonorthogonal terms in the pressure correction equation. *Numerical Heat Transfer*, *Part B* 1994; **26**:133–145.
7. Lehnhäuser T, Schäfer M. Improved linear interpolation practice for finite-volume schemes on complex grids. *International Journal for Numerical Methods in Fluids* 2002; **38**:625–645.
8. Demirdžić I, Perić M. Finite volume method for prediction of fluid flow in arbitrary shaped domains with moving boundaries. *International Journal for Numerical Methods in Fluids* 1990; **10**:771–790.
9. Durst F, Schäfer M. A parallel blockstructured multigrid method for the prediction of incompressible flow. *International Journal for Numerical Methods in Fluids* 1996; **22**:549–565.
10. Ferziger J, Perić M. *Computational Methods for Fluid Dynamics*. Springer, Berlin, 1996.
11. Rhie CM, Chow WL. Numerical study of the turbulent flow past an airfoil with trailing edge separation. *AIAA Journal* 1983; **21**:1525–1532.
12. Miller TF, Schmidt FW. Use of a pressure-weighted interpolation method for the solution of the incompressible Navier-Stokes Equations on a nonstaggered grid system. *Numerical Heat Transfer* 1988; **14**:213–233.
13. Moulinec C, Wesseling P. Colocated schemes for the incompressible Navier-Stokes equations on non-smooth grids for two-dimensional problems. *International Journal for Numerical Methods in Fluids* 2000; **32**: 349–364.
14. Stone H. Iterative solution of implicit approximations of multi-dimensional partial differential equations. *SIAM Journal on Numerical Analysis* 1968; **5**:530–568.

